Journal of Hazardous Materials 192 (2011) 361–367

Contents lists available at ScienceDirect

Journal of Hazardous Materials

journal homepage: www.elsevier.com/locate/jhazmat

NO treated TiO_2 as an efficient visible light photocatalyst for NO removal

Zhihui Ai[a,b,*], Linli Zhu[a], Shuncheng Lee[b], Lizhi Zhang[a,*]

[a] Key Laboratory of Pesticide & Chemical Biology of Ministry of Education, College of Chemistry, Central China Normal University, Wuhan 430079, PR China
[b] Department of Civil and Structural Engineering, Research Center for Environmental Technology and Management, The Hong Kong Polytechnic University, Hong Kong, PR China

ARTICLE INFO

Article history:
Received 23 January 2011
Received in revised form 18 April 2011
Accepted 12 May 2011
Available online 18 May 2011

Keywords:
Nitrogen doped TiO_2
NO
Photocatalysis
Visible light

ABSTRACT

In this study, we report that nitrogen doped TiO_2 could be achieved via thermal treatment of Degussa P25 TiO_2 in NO atmosphere directly (P25–NO). The samples were characterized with XRD, XPS, and FT-IR. The characterization results suggested that nitrogen species were interstitially doped in P25–NO during the NO thermal treatment process. In comparison with P25, the P25–NO exhibited significantly enhanced photocatalytic activities under visible light irradiation ($\lambda > 420$ nm) for gaseous NO removal. On the basis of electronic band structure theory, we proposed a possible mechanism for the enhanced visible light driven photocatalytic oxidation process over the interstitial N doping P25–NO samples. This work could not only deepen understanding of the enhanced photoactivity originated from interstitial N doping in TiO_2, but also provide a facile route to prepare nitrogen doped TiO_2 for environmental and energy applications.

1. Introduction

In recent years, increasing interest has been dedicated to photocatalysis owing to its potential applications in both environmental and energetic fields. TiO_2 has been the most important catalyst extensively employed in environmental remediation, photoelectrolysis of water, and in dye-sensitized solar cells because of being inexpensive, chemically stable, and nontoxic [1–4]. For TiO_2, the bottom of the conduction band and the top of the valence band consist of empty Ti^{4+} d orbitals and O 2p atomic orbitals, respectively. As is well-known, the electron (e^-)–hole (h^+) pairs are generated when TiO_2 is irradiated by photons with an energy greater than or equal to the band gap energy, and these charge carriers can then migrate to the surface to initiate various redox reactions of the adsorbates through some reactive species, such as the photogenerated e^- and h^+, superoxide ($^{\bullet}O_2^-$), and hydroxyl radical ($^{\bullet}OH$). However, with a band gap of 3.0–3.2 eV, TiO_2 can only absorb relatively little (4–5%) of the solar spectrum. Therefore, considerable efforts have been made to extend the absorption of TiO_2 into the visible light region by using doping technique [5]. Cationic dopants may result in localized d-levels deep in the band gap of TiO_2, which often serve as recombination centers for photogenerated charge carriers [4–6]. Thus, anion doping is a more appropriate method for the enhancement of visible light photoactivity, because the related impurity states of anion ions are supposed to be close to the valence band maximum. Recently, a growing number of publications reported the doping of TiO_2 with anions such as nitrogen, carbon, sulfur, and fluorine [7–11]. Among these anion approaches, nitrogen doped TiO_2 (N–TiO_2) in particular has received the greatest attention [12–17].

The visible light response for N–TiO_2 was first reported by Sato. He attributed the sensitization of the visible light to the NO_x impurity [18]. Later Asahi et al. [1] reported that N doping could reduce the band gap via the hybridzation of N 2p with the O 2p states. Since then, the enhanced visible light photocatalytic activity of N–TiO_2 was usually attributed to the decrease of the band gap through hybridization of the N 2p states with O 2p states on the top of the valence band [1] or the creation of a N-induced mid gap level just above the O 2p valence band maximum (VBM) [15,19]. However, recent electronic structure calculation indicated that there was virtually no shift of the upper edge of the O 2p valence band for the nitrogen doped TiO_2. Instead, occupied N 2p localized states appeared slightly above the valence band edge [20]. Among current debates on the mechanistic explanation of the nitrogen species in N–TiO_2 materials, two main mechanisms were generally proposed and accepted. One involves substitutional doping where O atoms are partially substituted by N atoms [21]. The other is interstitial doping, in which N species are located in interstitial sites [12]. In the substitutional model, as the nitrogen atom is bound to three Ti atoms and replaces lattice oxygen in TiO_2, this nitrogen atom is in a negative oxidation state, giving the covalent character of the bond [1,22]. In the interstitial model, the nitrogen atoms are bound to one or more oxygen atoms and therefore are in a positive oxida-

* Corresponding authors at: Key Laboratory of Pesticide & Chemical Biology of Ministry of Education, College of Chemistry, Central China Normal University, Wuhan 430079, PR China. Tel.: +86 27 6786 7535; fax: +86 27 6786 7535.
E-mail addresses: jennifer.ai@mail.ccnu.edu.cn (Z. Ai), zhanglz@mail.ccnu.edu.cn (L. Zhang).

0304-3894/$ – see front matter © 2011 Elsevier B.V. All rights reserved.
doi:10.1016/j.jhazmat.2011.05.033

tion state which could range from the typical state of a hyponitrite species (NO^-) to that of nitrite (NO_2^-) and nitrate species (NO_3^-) [12,23].

There are usually four methods reported for the synthesis of N–TiO_2: (1) sputtering and implantation techniques [24]; (2) high-temperature sintering of TiO_2 under nitrogen-containing atmospheres generated by ammonia and urea [12,13]; (3) solution-based strategies such as precipitation, sol–gel, and solvothermal treatment [14,16,17]; and (4) direct oxidation of the dopant-containing titanium precursors (such as TiN) [16]. The parameters of preparation methods, starting Ti precursors, and nitrogen sources strongly affect nitrogen species in the resulting N–TiO_2, and therefore influence the final photocatalytic activities. Herein we report a new and facile approach to prepare nitrogen doped TiO_2 via thermal treatment of commercial P25 in NO atmosphere for the first time. We systematically characterize the resulting nitrogen doped TiO_2 and explore the reason for of its enhanced visible light photoactivity.

2. Experimental

2.1. Sample preparation

TiO_2 (P25, Degussa, Germany) was obtained from Sigma Hong Kong. All reagents were used without further purification. The N–TiO_2 samples were prepared by thermal treatment of P25 in a tubular furnace equipped with a gas flow controller in NO atmosphere. Typically, 1 g of P25 powder was loaded in a ceramic crucible, and then placed into the middle of quartz tube, which was connected to the NO atmosphere. The NO gas was acquired from a compressed gas cylinder at a concentration of 48 ppm NO (N_2 balance, BOC gas) with traceable National Institute of Stands and Technology (NIST) standard. The initial concentration of NO was diluted to 10 ppm by the air stream supplied by a zero air generator (Thermo Environmental Inc. model 111). N–TiO_2 samples were obtained by NO treatment of P25 at temperatures ranging from 500 to 700 °C for 2 h. The temperature was slowly increased and cooled down at a rate of 3 °C/min during the heating and cooling process. After cooling to room temperature, the samples were taken out for further investigations. The as-prepared samples obtained at 500, 600, and 700 °C were labeled as P25–NO-500, P25–NO-600, and P25–NO-700, respectively. For comparison, P25 was also thermally treated in pure N_2 atmosphere at 500 °C for 2 h, the obtained sample was labeled as P25–N_2-500.

2.2. Characterizations

X-ray diffraction (XRD) patterns were obtained on a Bruker D8 Advance X-ray diffractometer with Cu Kα radiation (λ = 1.54178 Å). X-ray photoemission spectroscopy (XPS) with Al Kα source ($h\nu$ = 1486.6 eV) operated at 150 W (15 kV, 10 mA) (XPS: Thermo ESCALAB 250, USA) was used to investigate the surface properties and to probe the total density of the state (DOS) distribution in the valence band. The shift of the binding energy due to relative surface charging was corrected using the C1s level at 284.8 eV as an internal standard. Raman spectra were collected in a LabRAM HR High Resolution 880 UV Confocal Raman Microscope. For the measurements, a green laser (He–Ne 532.14 nm), 600 line/mm, 100× objective, 20 mW, and 100 μ pinhole was used. FT-IR spectra were recorded on a Nicolet Nexus spectrometer with the standard KBr pellet method. UV–vis diffuse reflectance spectra (DRS) were recorded at room temperature with the Cary 300 UV–vis spectrophotometer equipped with an integrated sphere. The nitrogen adsorption and desorption isotherms at 77 K were measured using a Micrometritics ASAP2010 system after samples were vacuum-dried at 473 K overnight.

2.3. Photocatalytic NO removal experiments

The photocatalytic experiments of NO removal were performed at ambient temperature in a continuous flow reactor. The volume of the rectangular reactor which was made of stainless steel and covered with saint-glass was 4.5 L (10 cm × 30 cm × 15 cm ($H \times L \times W$)). One sample dish (diameter, 12 cm) containing the 0.1 g of sample was placed in the middle of the reactor. A 300 W commercial tungsten halogen lamp (General Electric) was used as the simulated solar-light source. The lamp was vertically placed outside the reactor above the sample dish and a glass filter was placed to remove light below 420 nm. To obtain visible light, we remove the UV light with a glass filter, whose transmissivity of the UV zone (200–420 nm) was less than 1%. Four mini-fans were fixed around the lamp to avoid the temperature rise of the flow system. The NO gas was acquired from a compressed gas cylinder at a concentration of 48 ppm NO (N_2 balance, BOC gas) with traceable National Institute of Stands and Technology (NIST) standard. The initial concentration of NO was diluted to about 400 ppb by the air supplied by a zero air generator (Thermo Environmental Inc. model 111). The desired humidity level of the NO flow was controlled at 70% (2100 ppmv) by passing the zero air streams through a humidification chamber. The gas streams were premixed completely by a gas blender, and the flow rate was controlled at 4 L min^{-1} by a mass flow controller. After the adsorption–desorption equilibrium among water vapor, gases, and photocatalysts was achieved, the lamp was turned on. The concentration of NO was continuously measured by a chemiluminescence NO analyzer (Thermo Environmental Instruments Inc. model 42c), which monitors NO, and NO_2 with a sampling rate of 0.7 L/min. The reaction of NO with air was ignorable according to the results of control experiments in dark or under visible light in the absence of photocatalyst. The removal efficiency (η) of NO was calculated as Eq. (1):

$$\eta(\%) = \left(1 - \frac{C}{C_0}\right) \times 100\% \quad (1)$$

where C and C_0 were the concentrations of NO in the outlet stream and the feeding stream, respectively.

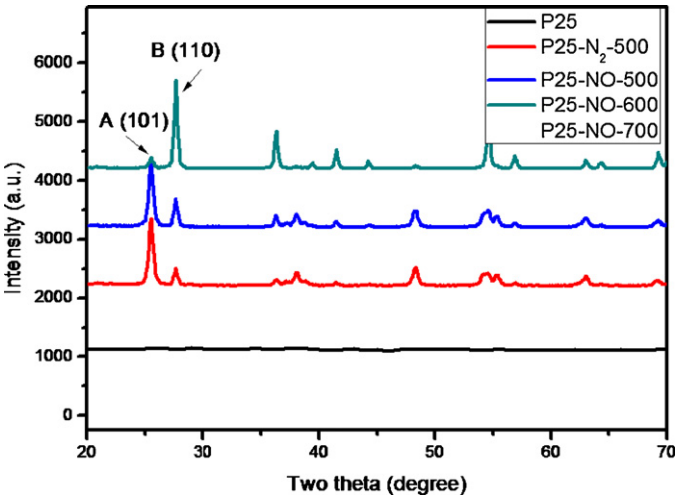

Fig. 1. XRD patterns of P25, P25–N_2-500, and the P25–NO samples obtained at different temperature.

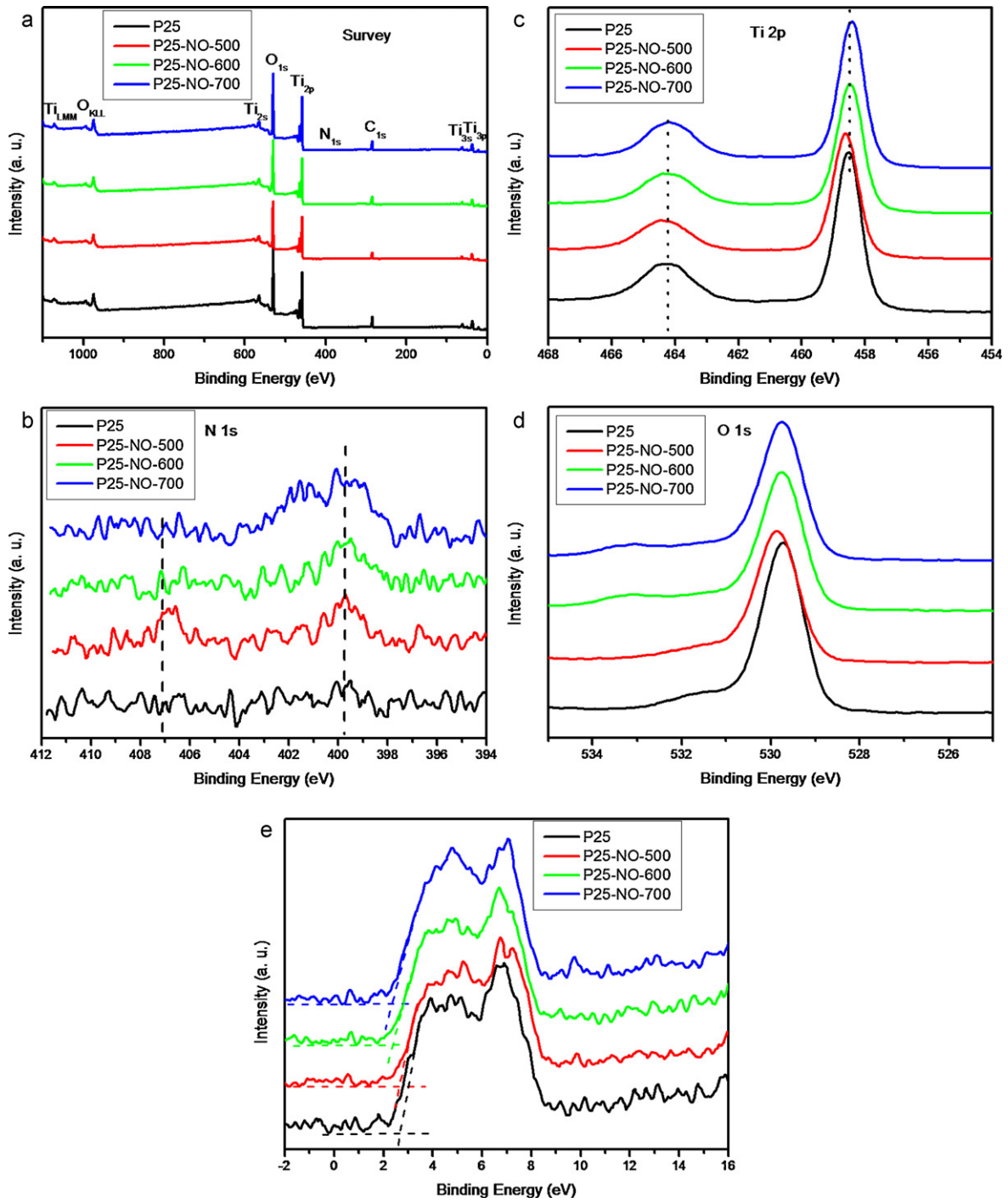

Fig. 2. XPS spectra of P25 TiO_2 and the as-prepared P25–NO samples: (a) survey; (b) high resolution XPS of N1s; (c) Ti 2p; (d) O1s; and (e) valence band XPS spectra.

3. Results and discussion

3.1. Characterization

The XRD patterns of pure P25 and the as-prepared N–TiO_2 can be indexed to TiO_2 in the anatase and rutile phases (Fig. 1). The phase content of the samples can be calculated from the integrated intensities of anatase (1 0 1), rutile (1 1 0) and brookite (1 2 1) peaks according to Zhang and Banfield's report (Eqs. (2–4)) [25].

$$W_A = \frac{k_A A_A}{k_A A_A + A_R + k_B A_B} \quad (2)$$

$$W_R = \frac{A_R}{k_A A_A + A_R + k_B A_B} \quad (3)$$

$$W_B = \frac{k_B A_B}{k_A A_A + A_R + k_B A_B} \quad (4)$$

In Eq. (2–4), W_A, W_R, and W_B represent the weight fractions of anatase, rutile, and brookite, respectively. A_A, A_R, and A_B are the integrated intensities of anatase (1 0 1), rutile (1 1 0), and brookite (1 2 1) peaks, respectively. The variables k_A and k_B are two coefficients. It was reported that $k_A = 0.886$ and $k_B = 2.721$ [25]. Anatase and rutile in P25 were calculated to be 81.4% and 18.6%, respectively. The estimated phase contents of anatase and rutile in

P25–NO-500 are 80.7% and 19.3%, respectively. As higher thermal treatment temperature could lead to the transformation of anatase to rutile, P25–NO-600 consisted of about 72.9% of anatase and 27.1% of rutile, while the content of rutile was further increased to 90.5% in P25–NO-700.

The survey XPS spectra reveal that all samples are mainly composed of elements of Ti, O, and C (Fig. 2a). The carbon peak at around 284.5 eV could be attributed to the adventitious carbon on the surface of the sample [7,8,26]. We further measured the XPS spectra for the core level X-ray photoelectron spectroscopy (CL XPS) spectra of N1s region of the samples (Fig. 2b). No peak related to nitrogen was observed for P25. However, two clear peaks at the binding energies of around 400 eV and 407 eV were observed for P25–NO. Although the peak at 400 eV were obvious and broadening for all the P25–NO samples, the peaks located at 407 eV disappeared on the nitrogen doped TiO_2 samples with increasing thermal treatment temperature from 500 to 700 °C. The observed peaks at 400 eV are typical of interstitial N species doping N–TiO_2, which might be resulted from hyponitrite (NO^-) or nitrite (NO_2^-) or nitrate species (NO_3^-) [14,26,28]. The peaks at 407 eV further confirmed the existence of nitrite or nitrate species [14,27]. It is worth noting that the signal at around 396 eV could not be observed, suggesting the absence of substitutional N in the resulting N–TiO_2 samples. This result agrees with Sakthivel's observation. They observed a nitrogen peak around 404 eV, but did not find the signal at 396 eV [29]. A second peak at around 401 eV was observed in P25–NO-700 sample, while this feature is absent in the N1s spectra of P25 and other P25–NO samples. The peak at 401 eV could be assigned to the formation of substituted N in O–Ti–N at a high thermal treatment temperature of 700 °C (P25–NO-700) [30]. As shown in Fig. 2c, the binding energy of Ti $2p_{3/2}$ core level for P25 and P25–NO are located at 459 and 458 eV, respectively, implying the electronic interaction of Ti with anions is not obviously changed after the thermal treatment in NO atmosphere, suggesting that nitrogen was not incorporated into the TiO_2 lattice. Fig. 2d shows the O1s spectra of the samples. In comparison with that for P25, a broadening of the higher binding energy side around 533.5 eV is clearly observed for the P25–NO-600 and P25–NO-700 samples, suggesting the presence of another type of oxygen. This could be arisen from the presence of NO_x located in the interstitial sites. Recently, Rodriguez et al. [31] measured the XPS spectra of NO, NO_2, and NO_3 on a ZnO surface and found that the N1s peaks for NO and NO_2 were respectively located at 400 and 405 eV, while the O1s peak for –NO and –NO_2 was located at 533.5 eV, consistent with our result. Valence band XPS was further used for the observation of extra electronic states above the valence band of the samples (Fig. 2e). It can be seen that the valence band edge has exhibited red shift after nitrogen doping. Combined with core level XPS results, we conclude that the interstitial N states lies higher above the O2p valence band edge. This finding is consistent with the conclusion from recent literature reports [5,28].

Many researchers have proven that N–TiO_2 exhibit a dramatic improvement over pure TiO_2 in their optical absorption below 3.0 eV (usually in the range of 2.4–3.0 eV) as nitrogen incorporates into the TiO_2 lattice and effectively changes its electronic structure [1,12,13]. Comparing with P25, the P25–NO samples showed stronger absorption in the UV region (Fig. 3a). The absorption band gap energy, E_g, can be determined by the Kubelka–Munk function: $(\alpha h\nu)^n = A(h\nu - E_g)$, where $h\nu$ is the photoenergy, α is the absorption coefficient, A is a constant relative to the material, n decides the characteristics of the transition in a semiconductor. In our experiment, as TiO_2 is an indirect semiconductor, the energy band gaps could be estimated from the tangent line in the plot of the square root of Kubelka–Munk functions against photon energy. The tangent line, which is extrapolated to $(\alpha h\nu)^{1/2} = 0$, indicated that the band gaps obtained in plots of the $(\alpha h\nu)^{1/2}$ vs the energy of absorbed light were approximately 2.90, 2.90, 2.88 and 2.86 eV for the sample P25, P25–NO-500, P25–NO-600 and P25–NO-700, respectively (Fig. 3b). Among them, P25–NO-700 mainly constituted by rutile TiO_2 showed narrowest band gap. This is consistent with the fact that the resulting P25–NO samples are white in color. Similarly, Serpone and Kuznetsov also observed that N doping did not actually lead to a significant narrowing of the bandgap energy of the semiconductors in their studies [32,33]. In other words, the N dopants into TiO_2 does not lead to a significant narrowing of the bandgap energy of TiO_2, but increase the number of oxygen vacancies and defects, and therefore lead to enhanced absorption in the visible region [34]. It is worth noting that the absorption of the P25–NO-500 and P25–NO-600 samples in the $\lambda < 500$ nm region is enhanced (inset of Fig. 3a). This part of the absorption is thought to arise from additional N 2p mid gap band level above the valence band edge [35,36].

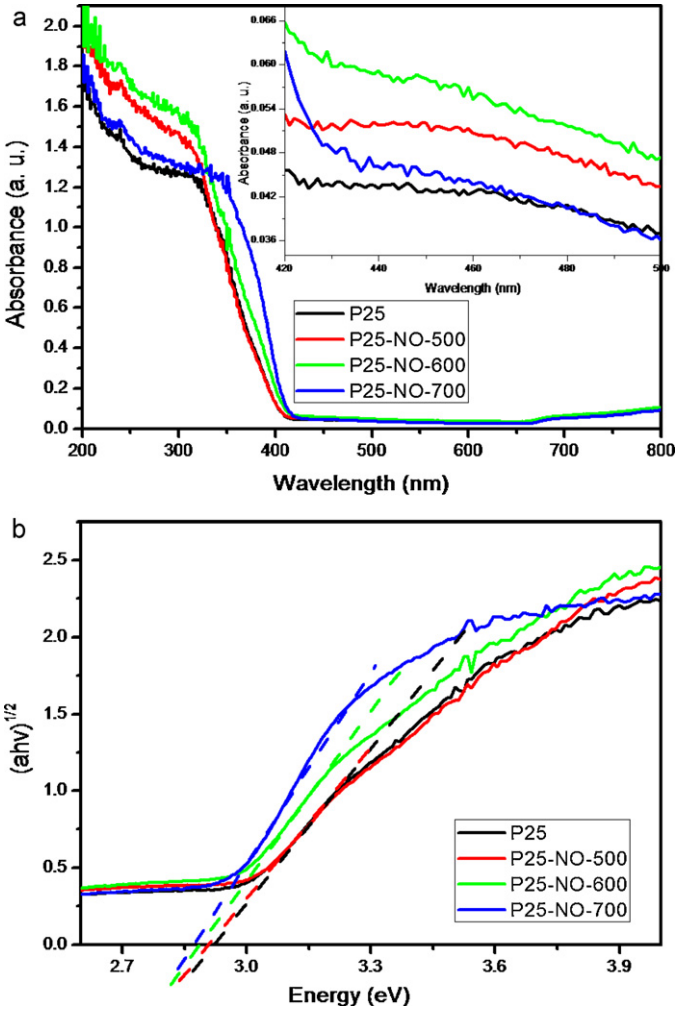

Fig. 3. (a) UV–vis diffuse reflectance spectra of P25 and the as-prepared P25–NO samples obtained at different temperature; the inset is the spectra in the range of 420–500 nm; (b) plots of the $(\alpha h\nu)^{1/2}$ vs the energy of absorbed light.

FT-IR was used to check the existence of nitrogen species on the surface of P25 during the thermal treatment process in NO atmospheres (Fig. 4). The IR spectra display broad bands at 3420 cm^{-1}, which are believed to be associated with the stretching vibrations of hydrogen-bonded surface water molecules and hydroxyl groups. The peak at 1640 cm^{-1} could be assigned to the bending vibrations of O–H group. The peak found at 2935 cm^{-1} could be associated with vibrations of C–H from the adventitious carbon on the surface of the samples. Comparing the spectra of the as-prepared P25–NO samples and P25, the bands at 1385, 1264, and 1050 cm^{-1}, imply-

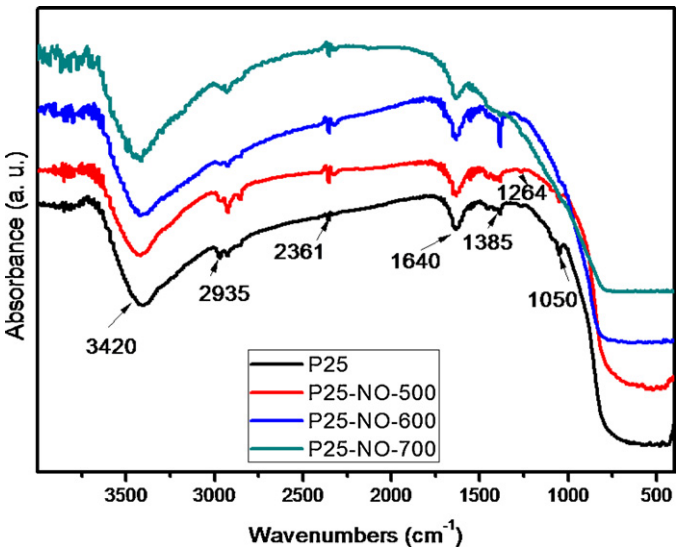

Fig. 4. FTIR spectra of P25 TiO_2 and the as-prepared P25–NO obtained at different temperature.

ing the existence of hyponitrite and nitrite groups [37], becomes stronger after the NO thermal treatment of P25. This further confirms the existence of nitrogen species.

3.2. Photocatalytic degradation of NO

The photocatalytic activities of P25, P25–NO, and P25–N_2-500 were measured through the photocatalytic removal of NO in gas phase (Fig. 5). It was found from Fig. 5 that NO could not be removed by direct photolysis under visible light irradiation without the presence of any photocatalysts. Fig. 5 shows that NO could even be photocatalytically oxidized on pure P25 under visible light irradiation. This is because P25 is a mixture consisting of anatase and rutile phase, the oxygen vacancy could thus be created at the boundaries of anatase and rutile grains, resulting in "oxygen deficiency doping" [38]. The photocatalytic activity of P25–N_2-500 is almost the same as that of pure P25, indicating that thermal treatment of P25 in N_2 atmosphere could not change its photoactivity under visible light. Impressively, P25–NO-500 and P25–NO-600 showed superior photocatalytic activity to P25 on degradation of NO under visible light. 36% and 35% of NO was photocatalytic oxidized on P25–NO-500

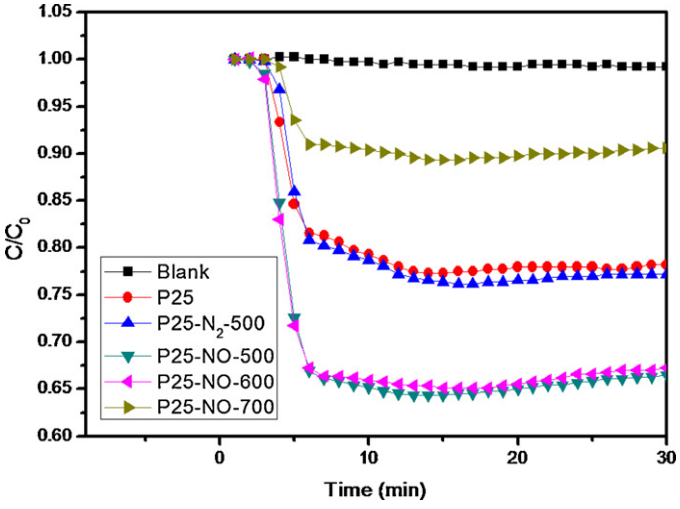

Fig. 5. Plots of the decrease in NO concentration vs irradiation time on different photocatalysts under visible light (λ > 420 nm).

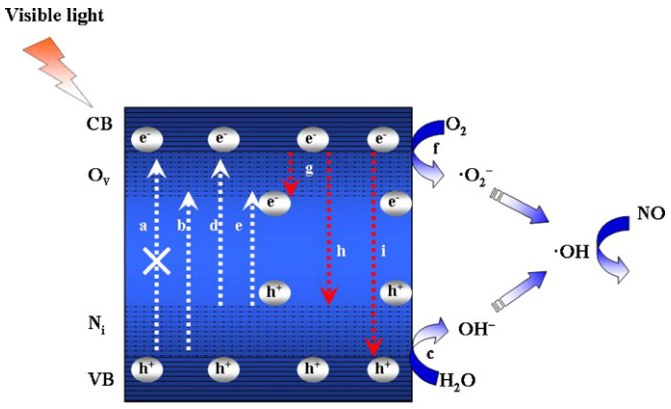

Scheme 1. Proposed band structure of interstitial nitrogen doped TiO_2 and the mechanism for visible light photocatalytic process.

and P25–NO-600 under visible light (λ > 420 nm) in 10 min of visible irradiation, respectively. These NO removal efficiencies were higher than that on the P25 (23%) and even superior to that of BiOBr nanoplate microspheres (30%) [39,40]. Nevertheless, higher thermal treatment temperature in NO atmosphere would decrease the activity of the sample. Only 11% of NO was oxidized on P25–NO-700 in 10 min of irradiation, this could be attributed to its lower BET surface area and more rutile TiO_2.

Generally, the overall photocatalytic activity of a semiconductor is primarily determined by three factors. The first is the surface area of the photocatalysts. Large surface area provides more surface sites for the adsorption of reactants molecules, making the photocatalytic process more efficient. The second is the photoabsorption ability in the available light energy region. More absorption in the visible region might enhance visible light-driven photocatalytic activity. The third is related to the separation and recombination rates of the photogenerated electrons and holes in the catalysts. The charge transfer and recombination are two competitive reaction pathways during the photocatalytic process, thus it is important to suppress the recombination rate and accelerate charge transfer to enhance the photocatalytic activity [40]. Nitrogen sorption was then used to measure the surface areas of the P25 and P25–NO samples, it was found that the BET surface areas of P25–NO-500 (23.1 m^2/g), P25–NO-600 (22.0 m^2/g), and P25–NO-700 (18.4 m^2/g) were lower than that of P25 (23.6 m^2/g), indicating that the photocatalytic activity enhancement of P25–NO-500 and P25–NO-600 could not be attributed to increased surface areas. Therefore, the enhanced visible light adsorption in the visible light region and charge separation could be the crucial factors for the photocatalytic activity enhancement of P25–NO-500 and P25–NO-600 samples.

The experimental evidence suggests interstitial nitrogen species are formed during the NO treatment process. Di Valentin et al. attributed visible light response to the occupied π^* character N–O localized states slightly above the valence band edge in interstitial N-doped anatase TiO_2 on the basis of their theoretical calculation [28]. Therefore, these nitrogen species occupied at interstitial sites of TiO_2 could give rise to a mid gap band level between valence and conduction bands [15,19] of the P25–NO-500 and P25–NO-600 samples, enabling them to absorb more light in the λ < 500 nm region and thus produce more photogenerated electrons and holes. Meanwhile, the interstitial nitrogen doped TiO_2 could lose oxygen to leave oxygen vacancies and electrons much easier than pure TiO_2 according to recent theoretical calculations and experimental results [5,12,14,35].

On the basis of above theory calculation and our experimental results, we proposed a possible band gap structure of P25–NO catalysts (Scheme 1). As shown in Scheme 1, if anatase or rutile TiO_2

do not possess any oxygen vacancies, the energy of visible light ($\lambda > 420$ nm) is not sufficient to excite electrons from the valence band to the conduction band, the process a cannot happen. Actually, there are many oxygen vacancies in the boundaries grains between its anatase and rutile phase in commercial P25, electrons can be excited from the valence band to the O vacancies (O_v) (process b), leaving holes at the valance band. These holes would react with surface adsorbed OH^- and water to produce $^\bullet OH$ radicals for NO oxidation (process c). This is the origin of the visible light photocatalytic activity of P25 [38]. As for P25–NO-500 and P25–NO-600, process b could take place. While for P25–NO-700, the process b would be retarded because of its main rutile TiO_2 phase, this is why the P25–NO-700 showed lowest photocatalytic activity on removal of NO under visible light. Meanwhile, because the interstitial nitrogen states (N_i) would be produced between valence and conduction bands in the interstitial nitrogen doping P25–NO samples, the electrons could thus be excited from the N_i to the conduction band (process d) or the O vacancies (process e) under visible light irrdiation. The additional processes (d and e) make the P25–NO samples easier excited under the visible light irradiation compared with P25. Therefore, both of the mid gap band level (N_i) and O vacancies (O_v) are responsible for the origin of visible light induced photocatalytic activity of NO treated P25, but only O vacancies (O_v) account for the visible light photocatalytic activity of untreated P25. There are four fates for these excited electrons: to react with H_2O to produce more $^\bullet OH$ radicals (process f) and to recombine with the holes in the N_i levels (process h) or the valance band (process i) as well as to be energetically favorably trapped by O_v (process g). According to Scheme 1, we proposed a possible visible light photocatalytic oxidation process of NO as follows. First, under visible light irradiation, electrons would be excited from the valance band of P25 to its O vacancies, or from the valance band and the N_i states mid gap band of P25–NO to their O vacancies and conduction bands, leaving holes in the valance band of P25 or in the valance band and N_i states mid gap band of P25–NO (Eq. (5)). H_2O adsorbed on the surface could produce surface hydroxyl groups (OH^-) and H^+ (Eq. (6)). Then, the holes and electrons will react with OH^- and molecule O_2 on the catalyst surface to form $^\bullet OH$ radicals and superoxide anion radicals ($^\bullet O_2{}^-$), respectively (Eq. (7)). The $^\bullet O_2{}^-$ radicals would then react with H_2O adsorbed to produce more $^\bullet OH$ radicals (Eq. (8)), which are known to be the most oxidizing species. Finally, these $^\bullet OH$ radicals react with gaseous NO. As can be seen from Eq. (7) that the surface hydroxyl groups accept holes generated by visible light irradiation to form hydroxyl radicals thus prevent electron–hole recombination. Therefore, it is expected that a greater number of hydroxyl groups yield a higher photocatalytic activity.

$$TiO_2 - N_i + vis \rightarrow h^+ + e_{CB}{}^- \quad (5)$$

$$H_2O \rightarrow OH_{(surf)}{}^- + H^+ \quad (6)$$

$$OH_{(surf)}{}^- + h^+ \rightarrow {}^\bullet OH \quad (7)$$

$$e_{CB}{}^- + O_2 \rightarrow {}^\bullet O_2{}^- \quad (8)$$

$$^\bullet O_{2(surf)}{}^- + H_2O \rightarrow {}^\bullet OH + OH^- \quad (9)$$

4. Conclusions

In summary, we have demonstrated a new and facile approach to prepare nitrogen doped TiO_2 via thermal treatment of commercial P25 in NO atmosphere for the first time. In comparison with that of P25, the NO treated P25 exhibited significantly enhanced photocatalytic activities under visible light irradiation ($\lambda > 420$ nm) for gaseous NO removal. On the basis of electronic band structure theory, we proposed a possible mechanism for the enhanced visible light driven photocatalytic oxidation process over the interstitial N doping P25 samples. This work could not only deepen understanding of the enhanced photoactivity originated from interstitial N doping in TiO_2, but also provide a facile route to prepare nitrogen doped TiO_2 for environmental and energy applications.

Acknowledgements

This work was supported by National Science Foundation of China (grants 20977039), Program for Distinguished Young Scientist of Hubei Province (grant 2009CDA014), Program for Innovation Team of Hubei Province (grant 2009CDA048), Self–Determine Research Funds of CCNU from the Colleges' Basic Research and Operation of MOE (grants CCNU09A02014, and CCNU09C01009), and National Basic Research Program of China (973 Program) (grant 2007CB613301).

References

[1] R. Asahi, T. Morikawa, T. Ohwaki, K. Aoki, Y. Taga, Visible-light photocatalysis in nitrogen-doped titanium oxides, Science 293 (2001) 269–271.
[2] X.L. Hu, G.S. Li, J.C. Yu, Design, fabrication, and modification of nanostructured semiconductor materials for environmental and energy applications, Langmuir 26 (2010) 3031–3039.
[3] X.F. Yang, J.L. Zhuang, X.Y. Li, D.H. Chen, G.F. Ouyang, Z.Q. Mao, Y.X. Han, Z.H. He, C.L. Liang, M.M. Wu, J.C. Yu, Hierarchically nanostructured rutile arrays. Acid vapor oxidation growth and tunable morphologies, ACS Nano 3 (2009) 1212–1218.
[4] J.G. Yu, Q.J. Xiang, M.H. Zhou, Preparation, characterization and visible-light-driven photocatalytic activity of Fe-doped titania nanorods and first-principles study for electronic structures, Appl. Catal. B Environ. 90 (2009) 595–602.
[5] A. Nambu, J. Graciani, J.A. Rodriguez, Q. Wu, E. Fujita, J.F. Sanz, N doping of TiO_2 [1 1 0]: photoemission and density-functional studies, J. Chem. Phys. 125 (2006), 094706-094706-8.
[6] I.C. Kang, Q.W. Zhang, S. Yin, T. Sato, F. Saito, Improvement in photocatalytic activity of TiO_2 under visible irradiation through addition of N–TiO_2, Environ. Sci. Technol. 42 (2008) 3622–3626.
[7] W.J. Ren, Z.H. Ai, F.L. Jia, L.Z. Zhang, X.X. Fan, Z.G. Zou, Low temperature preparation and visible light photocatalytic activity of mesoporous carbon-doped crystalline TiO_2, Appl. Catal. B Environ. 69 (2007) 138–144.
[8] Y. Huang, W.K. Ho, Z.H. Ai, X. Song, L.Z. Zhang, S.C. Lee, Aerosol-assisted flow synthesis of B-doped, Ni-doped and B–Ni-codoped TiO_2 solid and hollow microspheres for photocatalytic removal of NO, Appl. Catal. B Environ. 89 (2009) 398–405.
[9] Y. Huang, K.J. Deng, Z.H. Ai, L.Z. Zhang, Ultrasonic spray pyrolysis synthesis and visible light activity of carbon-doped $Ti_{0.91}Zr_{0.09}O_2$ solid solution photocatalysts, Mater. Chem. Phys. 114 (2009) 235–241.
[10] Y.W. Wang, Y. Huang, W.K. Ho, L.Z. Zhang, Z.G. Zou, S.C. Lee, Biomolecule-controlled hydrothermal synthesis of C–N–S-tridoped TiO_2 nanocrystalline photocatalysts for NO removal under simulated solar light irradiation, J. Hazard. Mater. 169 (2009) 77–87.
[11] W.K. Ho, J.C. Yu, S.C. Lee, Low-temperature hydrothermal synthesis of S-doped TiO_2 with visible light photocatalytic activity, J. Solid State Chem. 179 (2006) 1171–1176.
[12] O. Diwald, T.L. Thompson, T. Zubkov, E.G. Goralski, S.D. Walck, J.T. Yates, Photochemical activity of nitrogen-doped rutile TiO_2 [1 1 1] in visible light, J Phys. Chem. B 108 (2004) 6004–6008.
[13] J.L. Gole, J.D. Stout, C. Burda, Y.B. Lou, X.B. Chen, Highly efficient formation of visible light tunable $TiO_{2-x}N_x$ photocatalysts and their transformation at the nanoscale, J. Phys. Chem. 108 (2004) 1230–1240.
[14] M. Sathish, B. Viswanathan, R.P. Viswanath, C.S. Gopinath, Synthesis, characterization, electronic structure, and photocatalytic activity of nitrogen-doped TiO_2 nanocatalyst, Chem. Mater. 17 (2005) 6349–6353.
[15] T. Ihara, M. Miyoshi, Y. Iriyama, O. Matsumoto, S. Sugihara, Visible-light-active titanium oxide photocatalyst realized by an oxygen-deficient structure and by nitrogen doping, Appl. Catal. B Environ. 42 (2003) 403–409.
[16] S. Livraghi, M.R. Chierotti, E. Giamello, G. Magnacca, M.C. Paganini, G. Cappelletti, C.L. Bianchi, Nitrogen-doped titanium dioxide active in photocatalytic reactions with visible light: a multi-technique characterization of differently prepared materials, J. Phys. Chem. C 112 (2008) 17244–17252.
[17] X.F. Qiu, Y.X. Zhao, C. Burda, Synthesis and characterization of nitrogen-doped group IVB visible-light-photoactive metal oxide nanoparticles, Adv. Mater. 19 (2007) 3995–3999.
[18] S. Sato, Photocatalytic activity of NO_x-doped TiO_2 in the visible-light region, Chem. Phys. Lett. 123 (1986) 126–128.
[19] R. Nakamura, T. Tanaka, Y. Nakato, Mechanism for visible light responses in anodic photocurrents at N-doped TiO_2 film electrodes, J. Phys. Chem. C 108 (2004) 10617–10620.
[20] C. Di Valentin, E. Finazzi, G. Pacchioni, A. Selloni, S. Livraghi, M.C. Paganini, E. Giamello, N-doped TiO_2: theory and experiment, Chem. Phys. 339 (2007) 44–56.

[21] T. Morikawa, R. Asahi, T. Ohwaki, K. Aoki, Y. Taga, Band-gap narrowing of titanium dioxide by nitrogen doping, Jpn. J. Appl. Phys. Part 2 Lett. 40 (2001) L561–L563.
[22] M. Miyauchi, A. Ikezawa, H. Tobimatsu, H. Irie, K. Hashimoto, Zeta potential and photocatalytic activity of nitrogen doped TiO_2 thin films, Phys. Chem. Chem. Phys. 6 (2004) 865–870.
[23] Y. Sakatani, J. Nunoshige, H. Ando, K. Okusako, H. Koike, T. Takata, J.N. Kondo, M. Hara, K. Domen, Photocatalytic decomposition of acetaldehyde under visible light irradiation over La^{3+} and N co-doped TiO_2, Chem. Lett. 32 (2003) 1156–1157.
[24] A. Ghicov, J.M. Macak, H. Tsuchiya, J. Kunze, V. Haeublein, L. Frey, P. Schmuki, Ion implantation and annealing for an efficient N-doping of TiO_2 nanotubes, Nano Lett. 6 (2006) 1080–1082.
[25] H.Z. Zhang, J.F. Banfield, Understanding polymorphic phase transformation behavior during growth of nanocrystalline aggregates: insights from TiO_2, J. Phys. Chem. B. 104 (2000) 3481–3487.
[26] F. Dong, W.R. Zhao, Z.B. Wu, S. Guo, Band structure and visible light photocatalytic activity of multi-type nitrogen doped TiO_2 nanoparticles prepared by thermal decomposition, J. Hazard. Mater. 162 (2009) 763–770.
[27] P. Romero-Gomez, V. Rico, A. Borras, A. Barranco, J.P. Espinos, J. Cotrino, A.R. Gonzalez-Elipe, Chemical state of nitrogen and visible surface and schottky barrier driven photoactivities of N-doped TiO_2 thin films, J. Phys. Chem. C 113 (2009) 13341–13351.
[28] C. Di Valentin, G. Pacchioni, A. Selloni, S. Livraghi, E. Giamello, Characterization of paramagnetic species in N-doped TiO_2 powders by EPR spectroscopy and DFT calculations, J. Phys. Chem. B 109 (2005) 11414–11419.
[29] S. Sakthivel, H. Kisch, Photocatalytic and photoelectrochemical properties of nitrogen-doped titanium dioxide, Chemphyschem 4 (2003) 487–490.
[30] J. Fang, F. Wang, K. Qian, H.Z. Bao, Z.Q. Jiang, W.X. Huang, Bifunctional N-doped mesoporous TiO_2 photocatalyst, J. Phys. Chem. C 112 (2008) 18150–18156.
[31] J.A. Rodriguez, T. Jirsak, J. Dvorak, S. Sambasivan, D. Fischer, Reaction of NO_2 with Zn and ZnO: photoemission, XANES, and density functional studies on the formation of NO_3, J. Phys. Chem. B 104 (2000) 319–328.
[32] V.N. Kuznetsov, N. Serpone, Visible light absorption by various titanium dioxide specimens, J. Phys. Chem. B 110 (2006) 25203–25209.
[33] N. Serpone, Is the band gap of pristine TiO_2 narrowed by anion- and cation-doping of titanium dioxide in second-generation photocatalysts? J. Phys. Chem. B 110 (2006) 24287–24293.
[34] S.M. Prokes, J.L. Gole, X.B. Chen, C. Burda, W.E. Carlos, Defect-related optical behavior in surface-modified TiO_2 nanostructures, Adv. Funct. Mater. 15 (2005) 161–167.
[35] C. Di Valentin, G. Pacchioni, A. Selloni, Origin of the different photoactivity of N-doped anatase and rutile TiO_2, Phys. Rev. B 70 (2004) 19384–19387.
[36] Z.S. Lin, A. Orlov, R.M. Lambert, M.C. Payne, New insights into the origin of visible light photocatalytic activity of nitrogen-doped and oxygen-deficient anatase TiO_2, J. Phys. Chem. B 109 (2005) 20948–20952.
[37] S. Sakthivel, M. Janczarek, H. Kisch, Visible light activity and photoelectrochemical properties of nitrogen-doped TiO_2, J. Phys. Chem. B 108 (2004) 19384–19387.
[38] Z.Y. Zhao, Q.J. Liu, Mechanism of higher photocatalytic activity of anatase TiO_2 doped with nitrogen under visible-light irradiation from density functional theory calculation, J. Phys. D: Appl. Phys. 41 (2008) 025105.
[39] Y. Huang, W.K. Ho, S.C. Lee, L.Z. Zhang, G.S. Li, J.C. Yu, Effect of carbon doping on the mesoporous structure of nanocrystalline titanium dioxide and its solar-light-driven photocatalytic degradation of NO_x, Langmuir 24 (2008) 3510–3516.
[40] Z.H. Ai, W.K. Ho, S.C. Lee, L.Z. Zhang, Efficient photocatalytic removal of NO in indoor air with hierarchical bismuth oxybromide nanoplate microspheres under visible light, Environ. Sci. Technol. 43 (2009) 4143–4150.